Biophysical Journal, Volume 99

Supporting Material

FRAP Analysis of Membrane-Associated Proteins: Lateral Diffusion and Membrane-Cytoplasmic Exchange

Nathan W. Goehring, Debanjan Chowdhury, Anthony A. Hyman, and Stephan W. Grill

Supplemental Material

FRAP analysis of membrane-associated proteins: lateral diffusion and membrane-cytoplasmic exchange

Nathan W. Goehring, Debanjan Chowdhury, Anthony A. Hyman, and Stephan W. Grill

1 Schematic of 1-D and 2-D bleaching

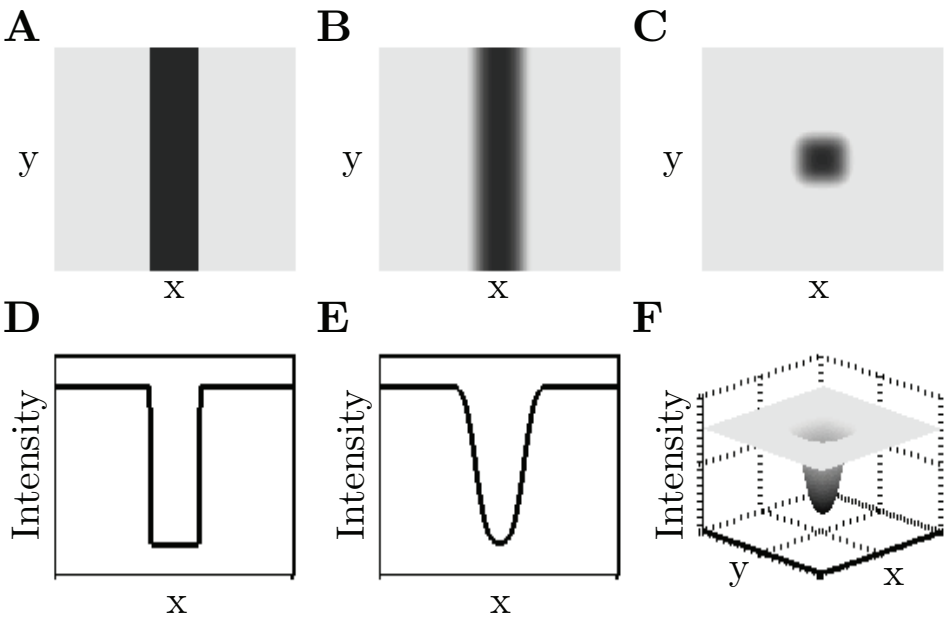

Figure S1. Schematic of bleach geometries. Examples of three bleach geometries: (*A*) an ideal sharp-edged stripe, (*B*) a stripe with smooth edges that take the form of error functions, and (*C*) a 2-D box with smooth edges. (*D-F*) Plots of fluorescence corresponding to the geometries shown in (*A-C*).

2 Simulating the effect of noise

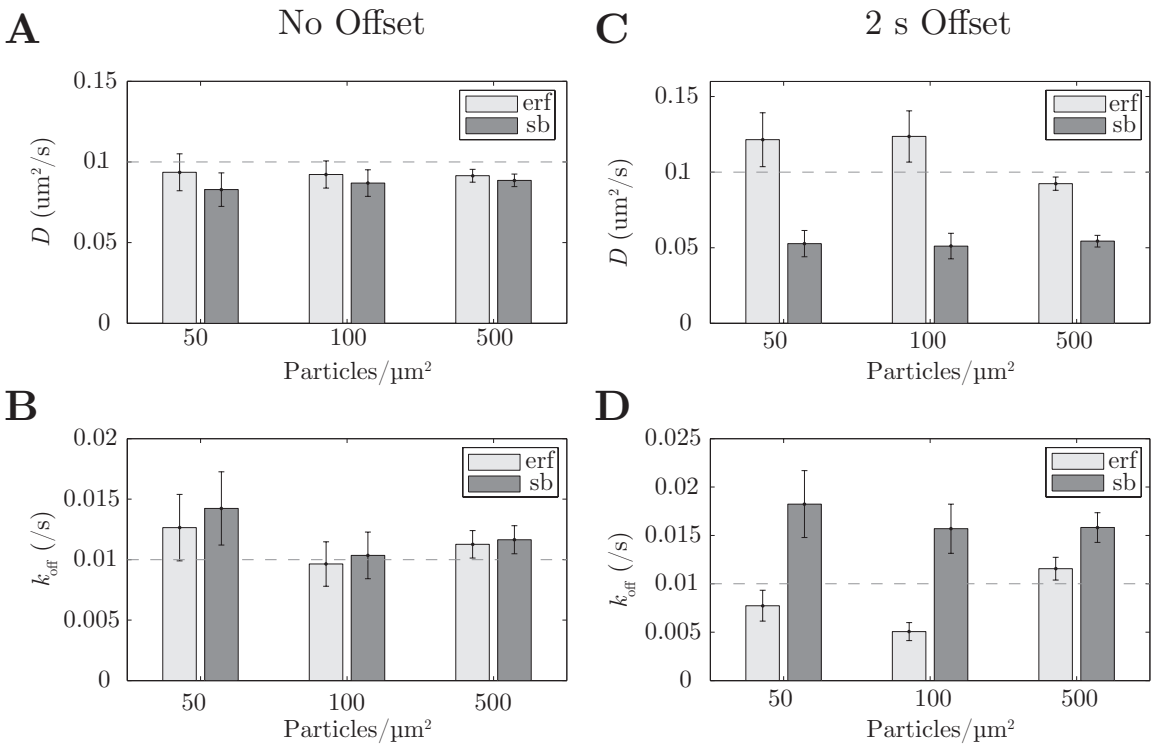

Figure S2. FRAP fitting is robust to noise. Simulations were performed as in Figure 1, but with particle densities 5-or 10-fold lower to increase stochastic fluctuations (n = 30). Fit values for D (*A, C*) and k_{off} (*B, D*) are shown for both the sharp (sb) and smooth (erf) box fit. For no bleach offset, both fits reproduce the expected values for both parameters well across all noise levels, although the spread of the data is higher for higher noise simulations (*A-B*). For a 2 s bleach offset (*C-D*), deviations arise for the higher noise cases (50, 100 particles / μm^2) for both sharp box and smooth box fits. For the smooth box case, these deviations arise due to increasingly difficulty in accurately fitting the shape of the edges of the bleach area boundaries (data not shown). Although the sharp box regime is not subject to this problem, this does not overcome its failure to account for lateral diffusion during the bleach offset, as we show in Figure 1, and the sharp box for the most part still leads to larger errors compared to the smooth box regime.

3 Additional tests of smooth vs. sharp box regimes

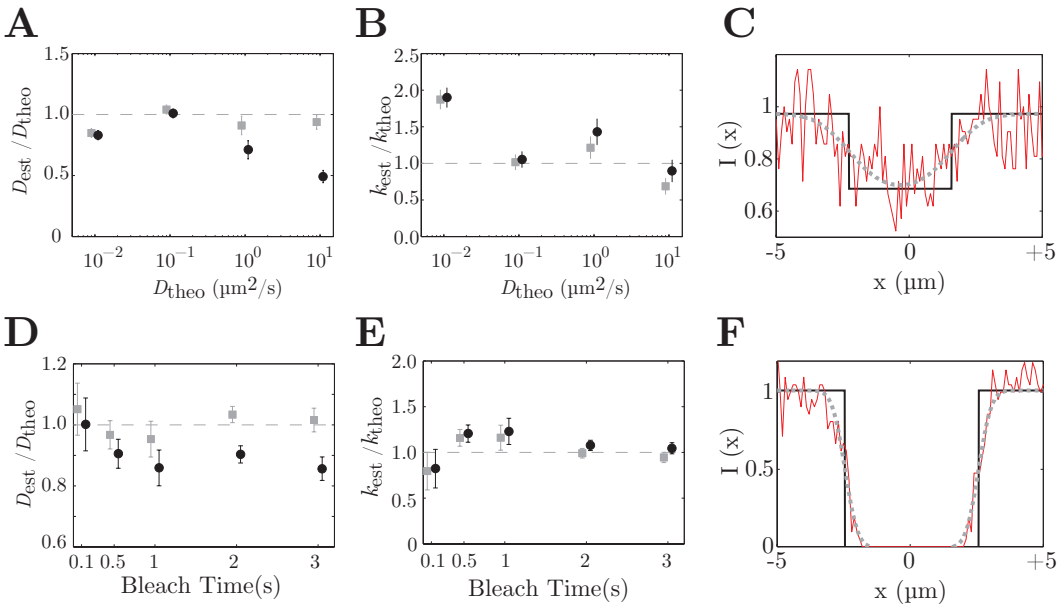

Figure S3. The *smooth box (erf)* model reduces errors associated with FRAP analysis for fast diffusing species and long bleach durations. In addition to changes in the bleach offset, we examined two additional conditions that can lead to significant deviations of the actual shape of the bleach region from an ideal box. These occur as a function of the ratio of the timescale of lateral diffusion and the timescales of bleaching and image acquisition. To explore these effects, we performed simulations in which we either (1) varied the diffusion coefficient, holding constant the ratio of D to k_{off}, the bleach duration, and the bleach offset (*A-C*), or (2) simply increased the bleach duration (*D-F*). In both cases, fitting with the sharp box regime leads to increasing errors in measurement of the diffusion coefficient (*A, D*). Using the smooth box regime reduces these errors significantly and results in as good or better measurement of k_{off}. Consistent with this result, the smooth box fit captures the initial fluorescence distributions in both cases much better (*C, F*). Intensity (*red line*), the sharp box fit (*solid black*) and smooth box fit (*dashed gray*) are shown. However, we should note that we still do not obtain perfect agreement in the measured and theoretical coefficients, with deviations of up to $5-10\%$ in our measurements of D, suggesting that there are likely remaining deviations in the fluorescence that are not fully captured by our parameterization. Because of the greater number of particles bleached in the simulations depicted in (*D-F*), these simulations were performed with 4-fold larger system (40×40 μm).

4 Analysis of a case of 2-D diffusion alone

To examine the behavior of our model in a case of pure diffusion, we performed FRAP on soluble GFP within a thin ($\sim 6\,\mu$m thick) film. Purified His-GFP (gift of D. Drexel) was suspended in 10 mM Tris, 1 mM EGTA, 0.1 mg/ml BSA plus 60% or 80% glycerol and mounted between a BSA coated slide and coverslip. Bleaching was performed as described in the Supplemental Methods, with the following changes: a 128×256 pixel area was imaged at 0.242 s intervals at resolutions of 0.131 or 0.237 μm/pixel; bleaching was for 0.242 s; and the pinhole was fully dilated (800 μm) to maximize bleach depth, giving rise to an essentially 2-D bleach geometry which can be analyzed using our method. As seen in Table S1, the measured diffusion coefficient of soluble GFP in 80% (w/w) glycerol solution is nearly identical for both bleach areas and essentially no difference is seen when the data is analyzed using a pure lateral diffusion model or a diffusion and exchange model. We should point out that the values for k_{off} obtained when using the combined model yield exchange timescales ($1/k_{\text{off}} > 600$ s) that are several orders of magnitude longer than the FRAP recoveries (typically $< 20s$) and thus are not significantly different from zero. For comparison, we repeated the analysis using a 60% glycerol solution, which, as expected, resulted in a significantly higher diffusion coefficient (approx. 4.3-fold increased).

Table S1. Diffusion of soluble GFP in a 2-D environment

Sample	**Area**	$\boldsymbol{D}$ (diffusion only)	$\boldsymbol{D}$ (diffusion/exchange)	$\boldsymbol{k}_{\text{off}}$(diffusion/exchange)
80% Glycerol	140μm	$1.5 \pm 0.21\,\mu\text{m}^2/\text{s}$	$1.5 \pm 0.21\,\mu\text{m}^2/\text{s}$	$4.3 \pm 6.7 \times 10^{-4}\,/s$
80% Glycerol	43μm	$1.5 \pm 0.13\,\mu\text{m}^2/\text{s}$	$1.4 \pm 0.13\,\mu\text{m}^2/\text{s}$	$1.6 \pm 1.6 \times 10^{-3}\,/s$
60% Glycerol	140μm	$7.1 \pm 1.4\,\mu\text{m}^2/\text{s}$	$6.5 \pm 1.3\,\mu\text{m}^2/\text{s}$	$1.2 \pm 2.8 \times 10^{-4}\,/s$

5 Diffusion of GFP::PH$_{\delta 1}$ in the cytoplasm

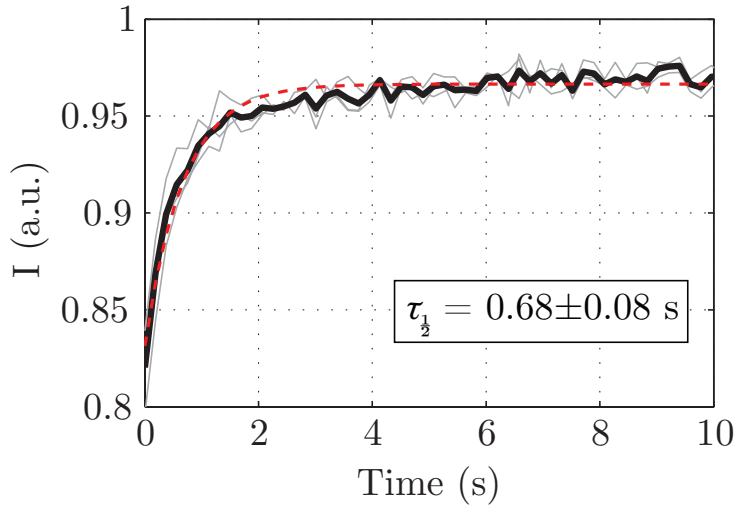

Figure S4. PH$_{\delta 1}$ diffuses rapidly in the cytoplasm. A 50 × 50 pixel square was bleached in the center of one cell embryos expressing GFP::PH$_{\delta 1}$ and intensity followed within a manually specified region. Because of low signal in the cytoplasm, five measurements for each embryo were pooled to generate individual traces. These individual traces (*gray lines*) and the mean recovery (*black line*) are shown along with a fit (*dashed red line*) to extract an approximate timescale for recovery (τ). To obtain a rough quantitation of this timescale, we used a simple exponential recovery of the form $I(t) = 1 - f_b\, e^{-t/\tau} + b$, where f_b is fraction bleached and b is an offset. We find that $\tau < 1\,s$. We should point out that our lateral diffusion model does not apply in the cytoplasm since bleaching in this environment using our configuration would give rise to a 3-D shape and require a more complex 3-D model to describe recovery. Rather, here we only intend to show the approximate recovery timescale.

6 Supplemental Methods

C. elegans strains and growth conditions

Worm stocks were maintained at 16°C and shifted to 25°C approximately 24 hours before analysis. Embryos were imaged at room temperature (22-25°C). Unless otherwise noted, embryos were dissected in 0.1 M NaCl, 4% sucrose, mounted on agarose pads, and sealed with VALAP. FRAP analysis of GFP::PH was performed on strain OD58 (*unc-119(ed3) III*; *ltIs38 [pAA1; pie-1/gfp::PH(PLC1δ1); unc-119 (+)]*) (S1) derived from Bristol N2.

Imaging and image analysis

FRAP was performed on an Olympus (Olympus Europa GmbH, Hamburg, Germany) FV-1000 system using a 60×/1.45 Oil UPlanSApo objective. A 128×128 pixel image was captured at 0.188 s intervals using a 488-nm laser line at 1% power and the pinhole set at 105 μm (back-projected pinhole diameter of approximately 250 μm). Following 20 prebleach frames, a 50x50 pixel region was bleached using 405 nm DPSS and 488-nm argon lasers at full power for 0.94 seconds (one scan iteration). Images were captured until no further recovery was evident. The size of the bleach region was altered using the built-in zoom function at 12×, 15×, and 20×, resulting in resolutions of 0.138, 0.110 and 0.087 μm/px, respectively.

Image stacks were loaded, and both the rough center of the bleach area and an appropriate unbleached reference area were selected manually. The center of the bleached spot, m_x, m_y, d_x, and d_y were obtained by fitting the x- and y-directions individually, and final fits inspected visually to prevent anomalous fits. These parameters were then used to define the 2-D error function (Eq. 11) that specified the boundaries of the bleached region to be analyzed. Mean fluorescence was monitored within this region as well as within the manually specified reference region to control for photobleaching. Individual recovery curves were normalized to the reference curves, and then to prebleach values. To reduce the effects of random fluctuations, individual curves were averaged before fitting with Eq. 12 using mean values for the ROI parameters obtained from the 2-D error function fit. To obtain an estimate of the error associated with these measurements, curves were fit individually and the associated standard error of the mean calculated. Fitting was done using Matlab (The Mathworks, Natick, MA). Sample scripts for analysis of 2-D bleach geometries are available as Supplemental Material from BJ online (http://www.biophysj.org/biophysj/supplemental/S0006-3495(10)01028-3). The most current versions can be found at the MPI-CBG website (http://publications.mpi-cbg.de/itemPublication.html?documentId=4142).

For fitting using a sharp box regime, we followed the above procedure and took the center and edges of the sharp box defined by d_x and d_y as above to limit the differences in the two regimes to the boundary effects. The normalized mean fluorescence recovery was then fit using Eq. S2 (see below).

Due to bleach geometry, the cytoplasmic pool of GFP::PH will necessarily be bleached.

However, this is unlikely to significantly affect our results. First, given the bleach period of 94 ms, only a small amount of this pool will be bleached. Second, the fluorescence in the cytoplasm is $\sim$ 8-fold lower than on the membrane (data not shown). Finally, both our data (Figure S4) and independent measurements using fluorescence correlation spectroscopy ($D =$ 8 μm^2/s) indicate cytoplasmic diffusion is rapid (S2). Thus, the assumption of a cytoplasmic concentration that is essentially uniform in space and time is a valid approximation.

Simulations

In order to generate simulated FRAP data for analysis, stochastic particle-based simulations of reversible membrane binding and lateral diffusion were performed in Matlab. Unless otherwise noted, diffusion and exchange was simulated over a 20×20 μm area at a particle density of $500/\mu$m^2 with 10 ms time steps. Also, unless otherwise specified, we assumed infinitely fast cytoplasmic diffusion and $k_{\text{on}} \gg k_{\text{off}}$. In this regime, particles that detach from the membrane immediately reattach at a random position. For bleaching, we specified a 4×4 μm $\text{ROI}_{\text{bleach}}$. Fluorophores were assumed to be inactivated at a fixed probability per unit time. In order to generate images for analysis, particle distributions were transformed into a 100×100 pixel image that was output as a TIFF file at 0.1 s intervals. Output TIFF stacks were then analyzed as described for the experimental FRAP curves. Simulation source-code is available from the authors on request.

To take into account, explicitly, the effects of a freely diffusing cytoplasmic pool, we considered the same planar system as above, but allowed molecules to switch between slow and fast diffusing states. The slow diffusing state corresponds to lateral diffusion in the membrane which is described by D. The fast diffusing state captures the effect of cytoplasmic diffusion and is described by D_{c}. Detachment and attachment to the membrane correspond to a switching between these two states, the kinetics of which is specified by the rate constants k_{on} and k_{off}. At steady state, the ratio $k_{\text{on}} \,/\, k_{\text{off}}$ will determine the relative fraction of the molecules in each of the two states. For illustration purposes, we let $k_{\text{on}} = k_{\text{off}}$ and thus $\sim 50\%$ of molecules will be in each state at a given time. Note that this simulation neglects diffusion orthogonal to the membrane. This is a reasonable model for cell geometries typically found in cell culture experiments where the cell is highly flattened on the substrate. For cells such as *C. elegans* embryos which have a spheroid geometry, this simplified pic-

ture will not be accurate and a full simulation would require a significantly more complex model. However, this model suffices to illustrate in a generic case how cytoplasmic recovery can affect FRAP results and how, by allowing for an initial period of recovery, the effect of cytoplasmic recovery on FRAP analysis can be minimized.

Recovery into a *sharp box*

As described, the initial condition given by Eq. 6 describes a bleached stripe with infinitely sharp borders. Solving Eq. 4 for $a_{sharp}(x,0)$ results in Eq. 7, which describes the time evolution of a sharp-edged bleach stripe. Solving for the recovery $I(t)$ for the normalized mean fluorescent recovery gives

$$I_{\text{sharp}}(t) = 1 + f_b \frac{2\ \mathrm{e}^{-k_{\text{off}}t}}{d_x}\left[\sqrt{\frac{Dt}{\pi}}\left(1-\mathrm{e}^{-d_x^2/(4Dt)}\right) - \frac{d_x}{2}\,\mathrm{erf}\left(\frac{d_x}{2\sqrt{Dt}}\right)\right]. \tag{S1}$$

Importantly, taking the limit of Eq. 10 for an infinitely sharp boundary ($m \to \infty$) results in the same solution.

Given this equivalence, in order to obtain the proper solution for a bleached square with infinitely sharp boundaries described by the following initial state

$$a_{\text{sharp}}(x,y,0) = \begin{cases} \frac{k_{\text{on}}^*}{k_{\text{off}}}(1-f_b) & (|x| < d_x/2 \ \text{ and } \ |y| < d_y/2) \\ \frac{k_{\text{on}}^*}{k_{\text{off}}} & (\text{otherwise}) \end{cases}$$

we take the limit of Eq. 12 as $m \to \infty$

$$\lim_{m\to\infty} I(t) = 1 - f_b \frac{4\ \mathrm{e}^{-k_{\text{off}}t}}{d_x d_y}\psi_{\text{sharp},x}(t)\psi_{\text{sharp},y}(t), \tag{S2}$$

where

$$\psi_{\text{sharp},i}(t) = \left[\sqrt{\frac{Dt}{\pi}}\left(\mathrm{e}^{-d_i^2/(4Dt)}-1\right) + \frac{d_i}{2}\mathrm{erf}\left(\frac{d_i}{2\sqrt{Dt}}\right)\right] \tag{S3}$$

and $i \in \{x, y\}$.

Supplemental References

S1. Audhya, A., F. Hyndman, I. X. McLeod, A. S. Maddox, J. R. Yates, A. Desai, and K. Oegema, 2005. A complex containing the Sm protein CAR-1 and the RNA helicase CGH-1 is required for embryonic cytokinesis in Caenorhabditis elegans. *The Journal of Cell Biology* 171:267–79.

S2. Petrásek, Z., C. Hoege, A. Mashaghi, T. Ohrt, A. A. Hyman, and P. Schwille, 2008. Characterization of protein dynamics in asymmetric cell division by scanning fluorescence correlation spectroscopy. *Biophys J* 95:5476–86.